Mon. Not. R. Astron. Soc. **000**, 1–8 (2012) Printed 27 February 2013 (MN LATEX style file v2.2)

A survey of lens spaces and large-scale CMB anisotropy

R. Aurich and S. Lustig
Institut für Theoretische Physik, Universität Ulm,
Albert-Einstein-Allee 11,
D-89069 Ulm, Germany

ABSTRACT
The cosmic microwave background (CMB) anisotropy possesses the remarkable property that its power is strongly suppressed on large angular scales. This observational fact can naturally be explained by cosmological models with a non-trivial topology. The paper focuses on lens spaces $L(p,q)$ which are realised by a tessellation of the spherical 3-space $\mathcal{S}^3$ by cyclic deck groups of order $p \leqslant 72$. The investigated cosmological parameter space covers the interval $\Omega_{\rm tot} \in [1.001, 1.05]$. Several spaces are found which have CMB correlations on angular scales $\vartheta \geqslant 60^\circ$ suppressed by a factor of two compared to the simply connected $\mathcal{S}^3$ space. The analysis is based on the S statistics, and a comparison to the WMAP 7yr data is carried out. Although the CMB suppression is less pronounced than in the Poincaré dodecahedral space, these lens spaces provide an alternative worth for follow-up studies.

Key words: Cosmology: theory, cosmic microwave background, large-scale structure of Universe

1 INTRODUCTION

Whole sky surveys of the cosmic microwave background (CMB) sky reveal a surprisingly low power in the anisotropy at large angular scales. This property was first discovered by Hinshaw et al. (1996) using the COBE measurements and was later substantiated by the WMAP observations (Spergel et al. 2003). Since multiconnected spaces possess a natural lower cut-off in their wave-number spectrum k, they generally have less CMB anisotropy power on large scales than spaces with infinite spatial volume. Because of this property they are interesting models for the explanation of the low CMB anisotropy power.

Multiconnected spaces can be generated by tessellating the simply connected space by identifying points u, u' that can be mapped $u \to u' = ug$ onto each other by applying transformations g belonging to a deck group Γ. Since this paper discusses only lens spaces $L(p,q)$, the simply connected space is the spherical 3-space $\mathcal{S}^3$. The topological spaces can also be written as $\mathcal{M} = \mathcal{S}^3/\Gamma$. An introduction to the cosmic topology is provided by Lachièze-Rey and Luminet (1995); Luminet and Roukema (1999); Levin (2002); Rebouças and Gomero (2004); Luminet (2008). The class of lens spaces $L(p,q) = \mathcal{S}^3/Z_p$ is specified by cyclic groups Z_p. The fundamental domains of the lens spaces can be visualised by a lens-shaped solid where the two lens surfaces are identified by a $2\pi q/p$ rotation for integers p and q that do not possess a common divisor greater 1 and obey $0 < q < p$. Therefore, there are in general several distinct cyclic groups Z_p which are characterised by the parameter q leading to distinct spaces $L(p,q)$ having the same group order p and thus the same spherical volume. For more restrictions on p and q, see below and Gausmann et al. (2001).

In the framework of cosmic topology, the lens spaces $L(p,q)$ are first studied by Uzan et al. (2004) but the CMB properties are not studied systematically. The lens spaces $L(p,q)$ with $p \leqslant 500$ and $q = 1$ are considered by Aurich et al. (2005), and it is found that this class does not provide models with a strong CMB suppression. The special case of group order $p = 8$ is investigated by Aurich et al. (2011). The lens space sequence $q = p/2 - 1$ is studied by Aurich and Lustig (2012).

The statistical CMB behaviour of the lens spaces $L(p,q)$ can be divided into two classes. The first class consists of the so-called homogeneous spaces for which the ensemble average of the CMB statistics with respect to the initial conditions is *independent* of the position of the CMB observer. The lens spaces $L(p,q)$ with $q = 1$ belong to this class. In contrast, the inhomogeneous spaces possess ensemble averages which depend on the position of the CMB observer. These models require a much more extensive CMB analysis since it does not suffice to select a single observer position and to compute the CMB statistics for this one position. Inhomogeneous spaces must be analysed for a large distribution of different observer positions in order to decide whether they provide admissible models according to the current cosmological observations. The lens spaces $L(p,q)$ with $q > 1$ are all inhomogeneous in this sense.

To elaborate this point, we have to introduce the de-

scription of the multiconnected spaces. The simply connected 3-space $\mathcal{S}^3$ is embedded in the four-dimensional Euclidean space described by the coordinates

$$\vec{x} \;=\; (x_0, x_1, x_2, x_3)^T \in \mathcal{S}^3$$

with the constraint $|\vec{x}\,| = 1$, i. e. the 3-space $\mathcal{S}^3$ is considered as the manifold with $x_0^2 + x_1^2 + x_2^2 + x_3^2 = 1$. Using complex coordinates $z_1 := x_0 + \mathrm{i}x_3$ and $z_2 := x_1 + \mathrm{i}x_2$, one can define the coordinate matrix

$$u \;:=\; \begin{pmatrix} z_1 & \mathrm{i}z_2 \\ \mathrm{i}\overline{z}_2 & \overline{z}_1 \end{pmatrix} \in \mathrm{SU}(2,\mathbb{C}) \equiv \mathcal{S}^3 \quad . \qquad (1)$$

Coordinate transformations can then be described as a matrix multiplication of the coordinate matrix u with a transformation matrix t. In the following the position of the observer is shifted by $u \to u' = ut$ using for the transformation matrix t the parameterisation

$$t(\rho,\alpha,\epsilon) \;=\; \begin{pmatrix} \cos(\rho)\, e^{+\mathrm{i}\alpha} & \sin(\rho)\, e^{+\mathrm{i}\epsilon} \\ -\sin(\rho)\, e^{-\mathrm{i}\epsilon} & \cos(\rho)\, e^{-\mathrm{i}\alpha} \end{pmatrix} \qquad (2)$$

with $\rho \in [0, \frac{\pi}{2}]$, $\alpha, \epsilon \in [0, 2\pi]$. It turns out that the CMB anisotropy depends only on the parameter ρ (Aurich et al. 2011; Aurich and Lustig 2012). The independence of the CMB statistics of the parameters α and ϵ is the advantage of the parameterisation (2) since it allows to study the variation of the statistical properties as a one-dimensional sequence of $\rho \in [0, \frac{\pi}{2}]$. Some of the lens spaces $L(p,q)$ possess the same CMB statistics for ρ and $\frac{\pi}{2} - \rho$. This allows to restrict the analysis to $\rho \in [0, \frac{\pi}{4}]$ for these spaces.

The lens spaces $L(p,q)$ and $L(p',q')$ are homeomorphic if and only if $p = p'$ and either $q = \pm q' (\mathrm{mod}\ p)$ or $q\,q' = \pm 1 (\mathrm{mod}\ p)$ (Gausmann et al. 2001). Two lens spaces $L(p,q)$ and $L(p,q')$ with $q\,q' = \pm 1 (\mathrm{mod}\ p)$ are usually considered as one model and only one of them is taken into account. It turns out, however, that the statistical properties of such two models are related so that the properties of the interval $\rho \in [0, \frac{\pi}{4}]$ of one model are identical to those of the interval $\rho \in [\frac{\pi}{4}, \frac{\pi}{2}]$ of the other model. In the following, we thus consider two such models as distinct but analyse their CMB statistic only on the restricted interval $\rho \in [0, \frac{\pi}{4}]$. The remaining models without such a partner are exactly those with the symmetry with respect to ρ and $\frac{\pi}{2} - \rho$. In this way, all possible values are computed by considering all models only for observer positions in $\rho \in [0, \frac{\pi}{4}]$.

Our simulations are based on cosmological parameters close to the concordance model. We use for the density parameter of the cold dark matter $\Omega_{\mathrm{cdm}} = 0.238$, for the density parameter of the baryonic matter $\Omega_{\mathrm{bar}} = 0.0485$, and for the Hubble constant $h = 0.681$. The density parameter of the cosmological constant Ω_Λ is varied so that the total density parameter Ω_{tot} is in the range $\Omega_{\mathrm{tot}} \in [1.001, 1.05]$. Therefore, the models are almost flat and possess only a slight positive curvature. In addition, the spectral index n_{s} is chosen to be $n_{\mathrm{s}} = 0.961$. The CMB code incorporates the full Boltzmann physics, e. g. the ordinary and the integrated Sachs-Wolfe effect, the Doppler contribution, the Silk damping and the reionisation are taken into account. The reionisation model of Aurich et al. (2008) is applied with the reionisation parameters $\alpha = 0.4$ and $\beta = 9.85$. The correlation function $C(\vartheta)$ and multipole moments C_l of lens spaces are computed along the lines given by Aurich and Lustig (2012).

2 CMB PROPERTIES OF LENS SPACES

As discussed in the Introduction, a main motivation for cosmic topology derives from the observed low power in the anisotropy at large angular scales. This suppression of CMB correlations on large angular scales is most clearly revealed by the temperature 2-point correlation function $C(\vartheta)$. It is defined as

$$C(\vartheta) \;:=\; \big\langle \delta T(\hat{n}) \delta T(\hat{n}') \big\rangle \quad \text{with} \quad \hat{n} \cdot \hat{n}' = \cos\vartheta \quad , \qquad (3)$$

where $\delta T(\hat{n})$ is the temperature fluctuation in the direction of the unit vector $\hat{n}$. The brackets $\langle \dots \rangle$ denote an averaging over the directions $\hat{n}$.

The large angular behaviour is probably at variance with the ΛCDM concordance model based on a space with infinite volume as emphasised by Aurich et al. (2008); Copi et al. (2009, 2010). The correlation $C(\vartheta)$ depends on the data from which it is derived and, therefore, it is relevant which mask is applied to the WMAP data. Copi et al. (2009) infer from their investigations that only 0.025% of realisations of the concordance model can describe the low correlations on separation scales greater than 60° in the WMAP data admitted by the KQ75 mask. It should be noted, however, that a reconstruction algorithm can be applied to estimate the masked sky regions and it is claimed by Efstathiou et al. (2010); Bennett et al. (2011) that there is no discordance to the ΛCDM concordance model in this case. In the following, we assume that the discordance is real (Aurich and Lustig 2011; Copi et al. 2011). This section is devoted to an analysis independent of observational data. In the next section the correlations of the lens spaces $L(p,q)$ are compared to the correlations obtained from the WMAP ILC 7yr map (Gold et al. 2011) without a mask and with the KQ85 7yr and KQ75 7yr masks.

The suppression of CMB power becomes obvious for angular scales above 60°. In order to quantify this observation by a scalar measure, the S statistics

$$S \;:=\; \int_{\cos(180^\circ)}^{\cos(60^\circ)} d\cos\vartheta\; |C(\vartheta)|^2 \qquad (4)$$

has been introduced by Spergel et al. (2003). Although this statistics eliminates the information about the correlation function $C(\vartheta)$, it has the advantage that different simulations of $L(p,q)$ can be compared by a single number.

For all lens spaces $L(p,q)$ with $p \leqslant 72$, the correlation function $C(\vartheta)$ is computed on a two-dimensional grid with the axes $\rho \in [0, \frac{\pi}{4}]$ and $\Omega_{\mathrm{tot}} \in [1.001, 1.05]$. The ρ interval is discretised by 101 equidistant points. For the Ω_{tot} interval, the step width $\Delta\Omega_{\mathrm{tot}} = 0.001$ is used on $[1.001, 1.03]$ and $\Delta\Omega_{\mathrm{tot}} = 0.002$ on $[1.03, 1.05]$. It would be desirable to use an even finer grid close to the $\Omega_{\mathrm{tot}} = 1.001$ border, but this is numerically too demanding. The mesh consists of 4040 grid points at which $C(\vartheta)$ is to be computed for each lens space leading to a total of 2,923,760 simulations that are to be analysed. From this grid, the best value for $S_{L(p,q)}(\Omega_{\mathrm{tot}}, \rho)$ is selected, which is the smallest one in order to get the maximal suppression in CMB power on angular scales with $\vartheta \geqslant 60^\circ$. We would like to note that the range $\Omega_{\mathrm{tot}} \in [1, 1.001]$ is not covered by our survey so that there is the possibility that some models selected at the border $\Omega_{\mathrm{tot}} = 1.001$ might be even better if smaller values of Ω_{tot} would be accessible. It turns out that there are indeed mod-

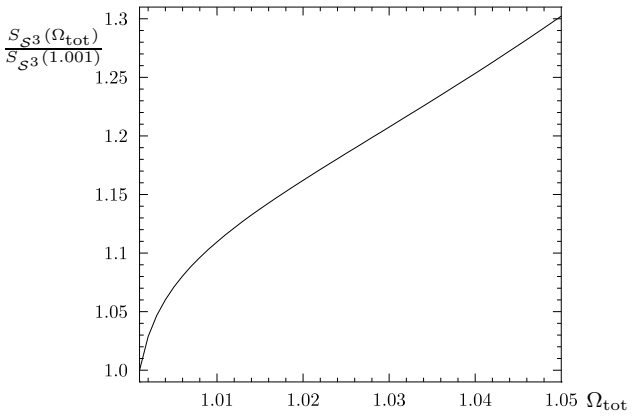

Figure 1. The difference in the normalisations of eqs. (5) and (6) is shown by plotting the ratio $S_{\mathcal{S}^3}(\Omega_{\rm tot})/S_{\mathcal{S}^3}(\Omega_{\rm tot}=1.001)$.

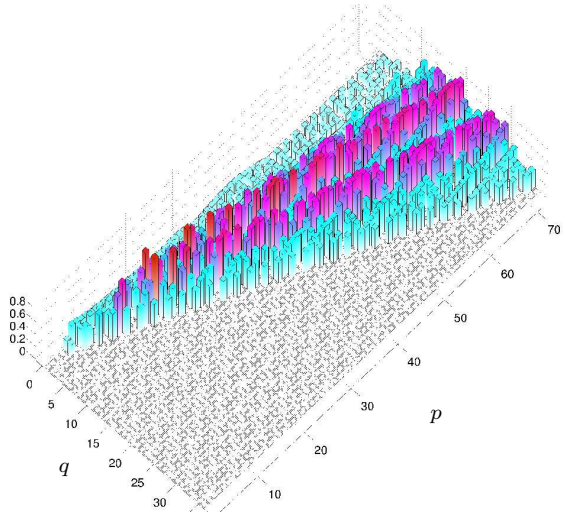

Figure 2. The minimum of the S_Ω statistics for the lens spaces $L(p,q)$ is extracted from the grid with axes $\rho \in [0, \frac{\pi}{4}]$ and $\Omega_{\rm tot} \in [1.001, 1.05]$. To emphasise small values of S_Ω, the height of the bins is proportional to $1/S_\Omega - 1$, i. e. larger bins correspond to smaller CMB power. Therefore, a value of zero indicates that the suppression of the CMB power is the same as for the simply connected $\mathcal{S}^3$ space. Note, that the S_Ω statistics is normalised to that of the simply connected 3-space $\mathcal{S}^3$ with the same $\Omega_{\rm tot}$.

els having their minimum at $\Omega_{\rm tot} = 1.001$. Such an example is given by the homogeneous lens spaces $L(p,1)$ where the minimum is at $\Omega_{\rm tot} = 1.001$ for $p \gtrsim 40$.

Before the minimum is searched, the $S_{L(p,q)}(\Omega_{\rm tot}, \rho)$ statistics is normalised in two different ways to the $S_{\mathcal{S}^3}(\Omega_{\rm tot})$ statistics of the simply connected 3-space $\mathcal{S}^3$. In the first procedure, $S_{L(p,q)}(\Omega_{\rm tot}, \rho)$ is normalised to the value of $S_{\mathcal{S}^3}(\Omega_{\rm tot})$ with the same $\Omega_{\rm tot}$, and then, the minimum is looked for

$$S_\Omega := \min_{\Omega_{\rm tot},\rho} \frac{S_{L(p,q)}(\Omega_{\rm tot}, \rho)}{S_{\mathcal{S}^3}(\Omega_{\rm tot})} \quad . \tag{5}$$

In the second procedure, $S_{L(p,q)}(\Omega_{\rm tot}, \rho)$ is normalised to the value of $S_{\mathcal{S}^3}(\Omega_{\rm tot})$ taken at $\Omega_{\rm tot} = 1.001$ leading to

$$S_\Lambda := \min_{\Omega_{\rm tot},\rho} \frac{S_{L(p,q)}(\Omega_{\rm tot}, \rho)}{S_{\mathcal{S}^3}(\Omega_{\rm tot} = 1.001)} \quad . \tag{6}$$

The first normalisation S_Ω emphasises the topological aspect since it compares the multiconnected space with the simply connected spherical 3-space $\mathcal{S}^3$ at the same value of $\Omega_{\rm tot}$. The second normalisation S_Λ can be considered as a comparison with the ΛCDM concordance model since $\Omega_{\rm tot} = 1.001$ is nearly indistinguishable from the flat case. The figure 1 displays the ratio $S_{\mathcal{S}^3}(\Omega_{\rm tot})/S_{\mathcal{S}^3}(\Omega_{\rm tot} = 1.001)$ in order to allow a comparison between the two statistics defined in eqs. (5) and (6).

Figure 2 provides an overview of the lens spaces $L(p,q)$ parameterised by the group order p and q together with their CMB suppression of correlations on large angles. In order to emphasise the positions (p,q) with small values of S_Ω, the height of the bins is chosen as $1/S_\Omega - 1$. Here, the value of S_Ω is the minimum found in the parameter range $\rho \in [0, \frac{\pi}{4}]$ and $\Omega_{\rm tot} \in [1.001, 1.05]$ for a given lens space $L(p,q)$. The figure reveals that, for fixed p, medium values of q provide in many cases models with a stronger CMB suppression than values close to $q = 1$ or to the maximal possible $q = p/2 - 1$. Since the angle $2\pi q/p$ is the angle by which the two surfaces of a lens have to be rotated relatively to each other before they are identified, the best CMB suppression is found for medium rotation angles. The best candidate lens spaces concentrate along the two lines with $q \simeq 0.28p$ and $q \simeq 0.38p$. This corresponds to rotation angles of 101° and 137° independent of the group order p.

The figure 2 is too complex in order to reveal the lens spaces $L(p,q)$ with the strongest CMB suppression. For that reason, the figures 3 and 4 show cross-sections of figure 2 so that the S_Ω dependence on the group order p can be inferred. Small values of S_Ω are favoured by the observations. The S_Ω statistics is shown for various values of q. Figures 3 and 4 show odd and even values of q, respectively. The values of q are distributed over the three panels in such a way that their curves do not entangle too much. There are several models $L(p,q)$ for which the CMB suppression is almost twice that of the simply connected spherical 3-space $\mathcal{S}^3$. The inspection of figure 3 reveals several q-curves with a significant CMB power suppression on large angular scales. For example, the $q = 9$ curve possesses two pronounced minima at $p = 23$ and $p = 32$. These two minima belong to the two diagonals $q \simeq 0.28p$ and $q \simeq 0.38p$ mentioned in the discussion of figure 2. The anisotropy measured by S_Ω is almost a factor 2 smaller than for the simply connected $\mathcal{S}^3$. However, one does not find a single lens space or at least a few candidates with a significant CMB suppression, but instead there are many lens spaces as received from the figures 3 and 4. A lot of models have values of S_Ω between 0.5 and 0.6. The table 1 lists the 10 lens spaces with the strongest CMB anisotropy suppression that are found on our $\Omega_{\rm tot}$-ρ grid. The $L(32,9)$ lens space belonging to the $q = 9$ curve is found at the sixth place in table 1. In addition, the table also gives the value of $\Omega_{\rm tot}$ and the observer position parameterised by ρ where the minimum is found.

The homogeneous lens spaces $L(p,1)$ do not possess a pronounced suppression of CMB power as revealed by the first panel of figure 3. Since the deck group consists only of Clifford translations for $q = 1$, the fundamental domain $\mathcal{F}$ defined as a Voronoi domain is independent of the observer position and so are the CMB properties (Aurich et al. 2011; Aurich and Lustig 2012). This is in contrast to the models

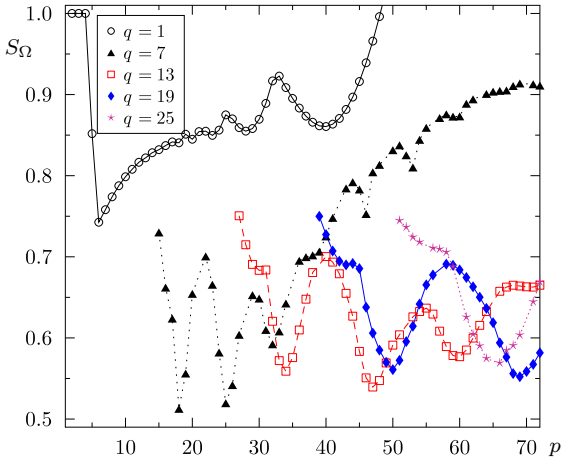

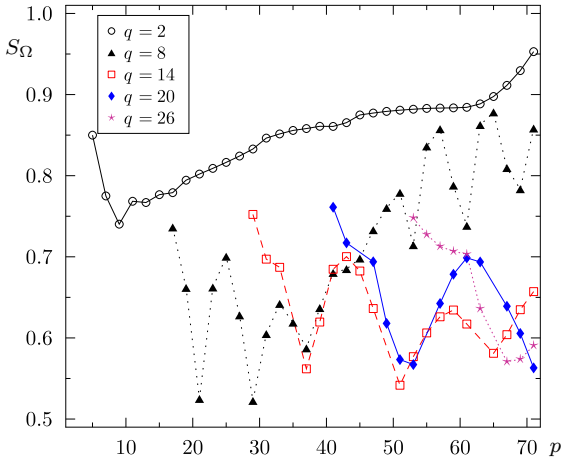

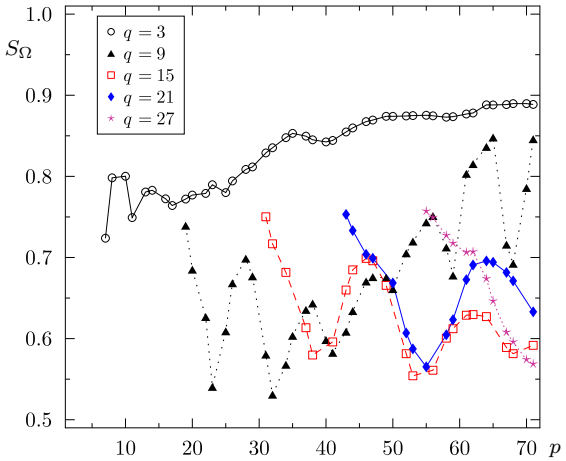

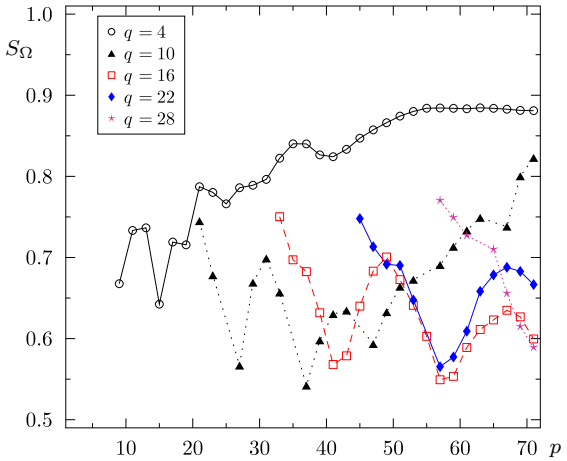

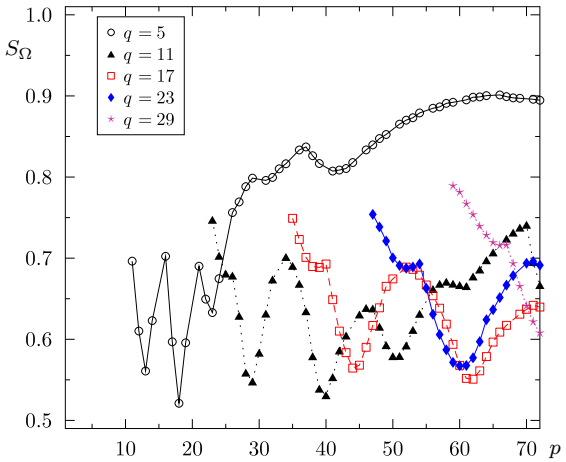

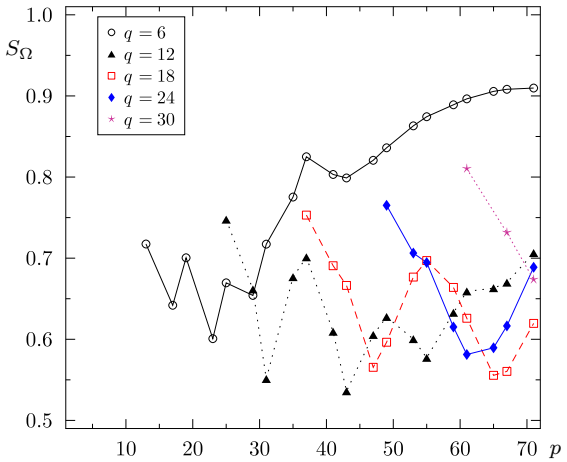

Figure 3. The S_Ω statistics is plotted for odd values of q as a function of the group order p.

Figure 4. The S_Ω statistics is plotted for even values of q as a function of the group order p.

with $q > 1$ which are all inhomogeneous. The absence of such a variability disfavours the homogeneous lens spaces $L(p, 1)$.

Up to now, the S_Ω statistics defined in eq. (5) is used which emphasises the topological aspect. The table 2 gives the ten best lens spaces $L(p, q)$ found on our grid, when the definition (6) is used. A comparison with table 1 lead to the conclusion that the application of the S_Λ statistics favours lens spaces $L(p, q)$ with a larger group order p and a smaller value of $\Omega_{\rm tot}$. This is caused by the fact that the S_Λ statistics compares the CMB correlations with that of the almost flat ΛCDM concordance model with $\Omega_{\rm tot} = 1.001$. This in turn favours models that are as flat as possible leading to a focus on spaces with a large group order p.

3 COMPARISON WITH THE WMAP DATA

The S statistics analysed in the previous section has the great advantage that it measures large scale correlations independent of observational data. The S statistics allows to find topological spaces with a CMB suppression on large angular scales. In this section, the correlation function $C(\vartheta)$ is compared with the correlation function obtained from the WMAP 7yr data (Gold et al. 2011). In order to compare the correlation function $C^{\rm model}(\vartheta)$ with the observed correlation function $C^{\rm obs}(\vartheta)$, the integrated weighted temperature correlation difference is introduced by Aurich et al. (2008)

$$I := \int_{-1}^{1} d\cos\vartheta \;\; \frac{(C^{\rm model}(\vartheta) - C^{\rm obs}(\vartheta))^2}{{\rm Var}(C^{\rm model}(\vartheta))} \qquad (7)$$

which tests all angular scales $\vartheta \in [0°, 180°]$. This is in contrast to the S statistics which focuses on the large angular range $\vartheta \geqslant 60°$. The variance is calculated by using

$${\rm Var}(C(\vartheta)) \;\approx\; \sum_l \frac{2l+1}{8\pi^2}\,[C_l\,P_l(\cos\vartheta)]^2 \quad . \qquad (8)$$

The correlation function $C^{\rm model}(\vartheta)$ is the ensemble average with respect to the Gaussian initial conditions. However, the ensemble average depends on the observer position.

The integrated weighted temperature correlation difference I is computed on the $\Omega_{\rm tot}$-ρ grid and the minimum $I_{\rm min}$ is determined in order to find the best simulation for each lens space. Now one has to specify the observational data on which $C^{\rm obs}(\vartheta)$ is based. As discussed at the beginning of section 2, the correlation function $C^{\rm obs}(\vartheta)$ depends significantly on the chosen mask that is applied to the WMAP ILC map. For that reason we compute $C^{\rm obs}(\vartheta)$ for three cases. In the first case $C^{\rm obs}(\vartheta)$ is computed from the whole WMAP ILC 7yr map that is without applying a mask. In the other two cases the two masks KQ85 7yr and KQ75 7yr are applied which are provided by Gold et al. (2011). The masks include 78.3% and 70.6% of the sky for the KQ85 7yr and KQ75 7yr masks, respectively.

The minima $I_{\rm min}$ of the I statistics computed from these three correlation functions $C^{\rm obs}(\vartheta)$ are presented in figures 5, 6, and 7, where the data are displayed for all lens spaces $L(p, q)$ up to group order $p = 72$. The values of $I_{\rm min}$ have to be compared with the value of the trivial topology, i. e. with the simply connected 3-space $\mathcal{S}^3 \equiv L(1, 1)$. The corresponding value can be read off from the case $p = 1$ and is shown as the straight horizontal line. All data points which

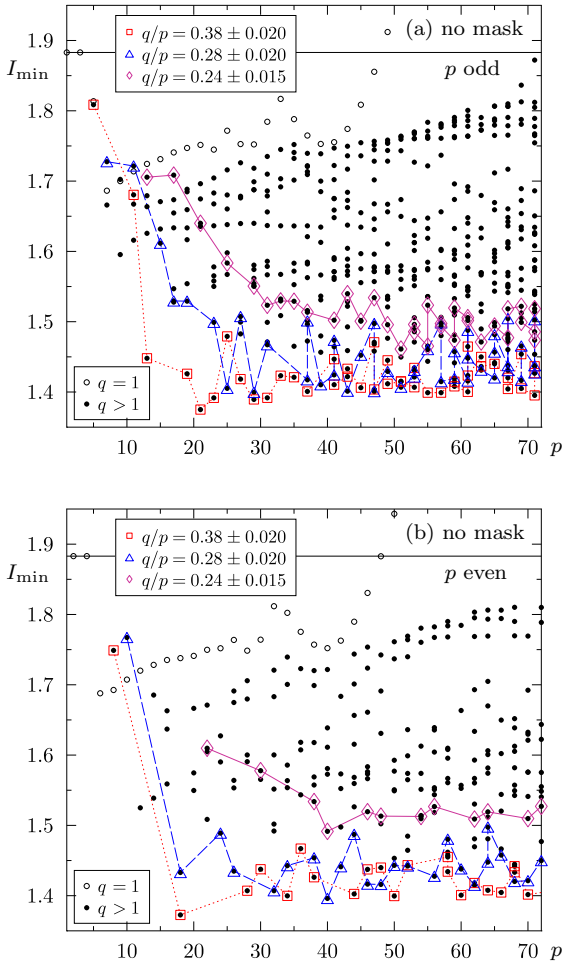

Figure 5. The minima $I_{\rm min}$ of the I statistics are plotted as a function of the group order p for each lens space $L(p, q)$. $C^{\rm obs}(\vartheta)$ is obtained from the full WMAP ILC 7yr map. The homogeneous lens spaces $L(p, 1)$ are shown as circles, and the inhomogeneous ones as full discs. In addition, the three sequences with $q/p = 0.38$, $q/p = 0.28$, and $q/p = 0.24$ are marked as squares, triangles, and diamonds, respectively. The panel (a) shows only lens spaces with an odd group order p, and panel (b) only those with an even group order p.

are below that of $\mathcal{S}^3 \equiv L(1, 1)$ describe the observed correlations better than the simply connected $\mathcal{S}^3$. All considered inhomogeneous lens spaces ($p \leqslant 72$) are thus preferred to the 3-space $\mathcal{S}^3$. In section 2 we found two sequences of lens spaces $L(p, q)$ with a superior suppression of large angle correlations. These two sequences with $q \simeq 0.38p$ and $q \simeq 0.28p$ are explicitly marked in figures 5, 6, and 7. It is seen that they also attract attention in the case of the I statistics. In addition to these two sequences, the figures also mark the sequence with $q \simeq 0.24p$, which leads for large group orders p to interesting models, if the KQ75 mask is applied.

The figures 5, 6, and 7 reveal a remarkable behaviour. Using no mask at all one observes in figure 5 that the best

Table 1. The lens spaces $L(p,q)$ with the largest suppression measured by S_Ω are listed together with the position in our $\Omega_{\rm tot}$-ρ grid.

$\mathcal{M}$	S_Ω	$\Omega_{\rm tot}$	ρ
$L(18,7)$	0.51260	1.044	0.43 $\pi/4$
$L(25,7)$	0.51954	1.034	0.48 $\pi/4$
$L(18,5)$	0.52109	1.050	0.58 $\pi/4$
$L(29,8)$	0.52235	1.027	0.43 $\pi/4$
$L(21,8)$	0.52481	1.034	0.37 $\pi/4$
$L(32,9)$	0.53090	1.023	0.39 $\pi/4$
$L(40,11)$	0.53111	1.016	0.33 $\pi/4$
$L(43,12)$	0.53594	1.014	0.31 $\pi/4$
$L(39,11)$	0.53915	1.016	0.32 $\pi/4$
$L(47,13)$	0.53946	1.011	0.27 $\pi/4$

Table 2. The lens spaces $L(p,q)$ with the largest suppression measured by S_Λ are listed together with the position in our $\Omega_{\rm tot}$-ρ grid.

$\mathcal{M}$	S_Λ	$\Omega_{\rm tot}$	ρ
$L(71,27)$	0.59506	1.003	0.09 $\pi/4$
$L(69,19)$	0.59575	1.005	0.17 $\pi/4$
$L(70,19)$	0.59836	1.005	0.17 $\pi/4$
$L(62,17)$	0.59970	1.007	0.22 $\pi/4$
$L(65,18)$	0.60023	1.006	0.20 $\pi/4$
$L(51,14)$	0.60026	1.009	0.24 $\pi/4$
$L(69,26)$	0.60055	1.003	0.09 $\pi/4$
$L(68,19)$	0.60073	1.006	0.20 $\pi/4$
$L(61,17)$	0.60079	1.007	0.22 $\pi/4$
$L(70,27)$	0.60082	1.003	0.09 $\pi/4$

models are around $p = 20$ with $I_{\rm min}$ below 1.4. This contrasts to the case with the largest mask, i. e. the KQ75 7yr mask with 70.6% sky coverage, where the smallest values of $I_{\rm min}$ occur at much larger group orders above $p = 50$, see figure 7. Surprisingly, the slightly smaller KQ85 7yr mask with 78.3% sky coverage is more similar to the case without a mask, since the smallest values of $I_{\rm min}$ are now at low group orders. Because of the severe dependence on the chosen mask, one can only conclude that the inhomogeneous lens spaces $L(p,q)$ describe the WMAP data better than the 3-space $\mathcal{S}^3$. But the data cannot be used to single out one or at least a few lens spaces $L(p,q)$ as best candidates.

4 SUMMARY

In this paper a class of topological spaces based on cyclic groups Z_p is investigated with respect to their CMB properties. These spaces are the lens spaces $L(p,q)$ of group order $p \leqslant 72$ which are realised in spherical spaces, i. e. with a positive spatial curvature. Only almost flat cosmological models are considered which belong to the interval $\Omega_{\rm tot} = [1.001, 1.05]$. Since the lens spaces $L(p,q)$ with $q > 1$ are inhomogeneous in the sense that the ensemble average of the CMB fluctuations is dependent on the position of the observer, a careful survey is required for each inhomogeneous lens space which takes this additional complication into account. For each space $L(p,q)$ with $p \leqslant 72$, the CMB correlations are computed for the above range of $\Omega_{\rm tot}$ and for a dense set of observer positions that exhausts the spatial CMB variability. From this set of almost 3 million simulations, the models with the lowest CMB correlations on large angular scales yield the interesting candidates.

The lens spaces $L(p,q)$ with $0 < q < p$ are distributed in the p-q plane within a triangular domain bounded by $q = 1$, i. e. the homogeneous spaces, and $q = p/2 - 1$. It turns out that models with a large CMB suppression on angular scales $\vartheta \geqslant 60^\circ$ concentrate on two bands which are approximately defined by $q \simeq 0.28p$ and $q \simeq 0.38p$. There are models within these two bands which have a CMB suppression for $\vartheta \geqslant 60^\circ$ being two times stronger than the simply connected spherical 3-space $\mathcal{S}^3$.

The correlations of the lens spaces $L(p,q)$ are compared with the WMAP 7yr data using the integrated weighted temperature correlation difference (7). Three correlation functions $C(\vartheta)$ are derived from the WMAP ILC 7yr map, based on the whole map and based on the data after applying the KQ85 7yr and KQ75 7yr masks. A number of lens spaces $L(p,q)$ are found which describe the three correlation functions $C(\vartheta)$ based on the WMAP data better than the 3-space $\mathcal{S}^3$. However, it turns out that for each of the three cases other best candidates are found. Because of the sensitivity on the admitted WMAP data, no firm conclusion can be drawn and no best candidate can be selected.

We thus conclude that there are lens spaces $L(p,q)$ with $q \simeq 0.28p$ and $q \simeq 0.38p$ which display a stronger CMB suppression on large angular scales than the simply connected space. Although the CMB suppression is less pronounced than in the Poincaré dodecahedral space, where the CMB correlation for $\vartheta \geqslant 60^\circ$ is reduced by a factor 0.11 at

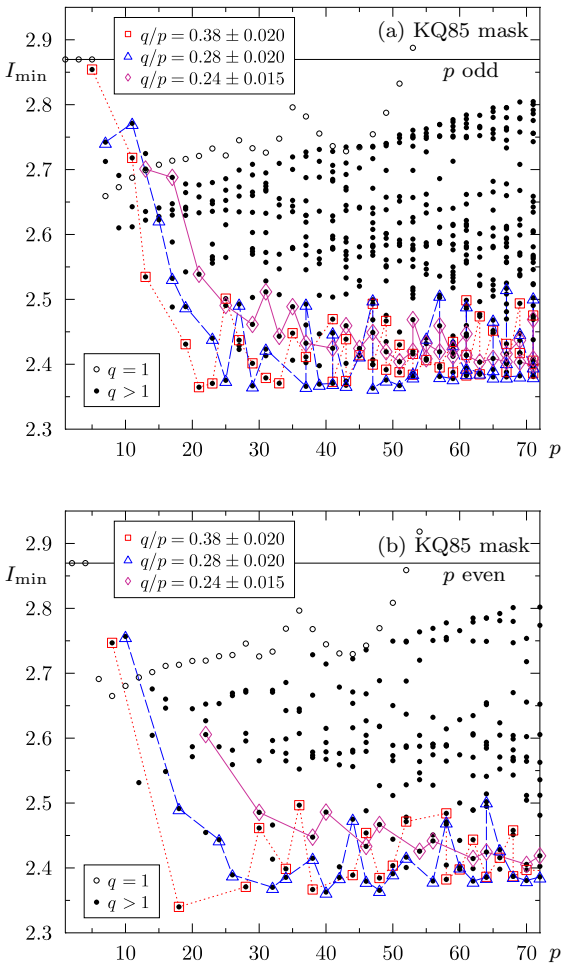

Figure 6. The minima $I_{\min}$ of the I statistics are shown as in figure 5. However, $C^{\text{obs}}(\vartheta)$ is obtained from the WMAP ILC 7yr map by applying the KQ85 mask.

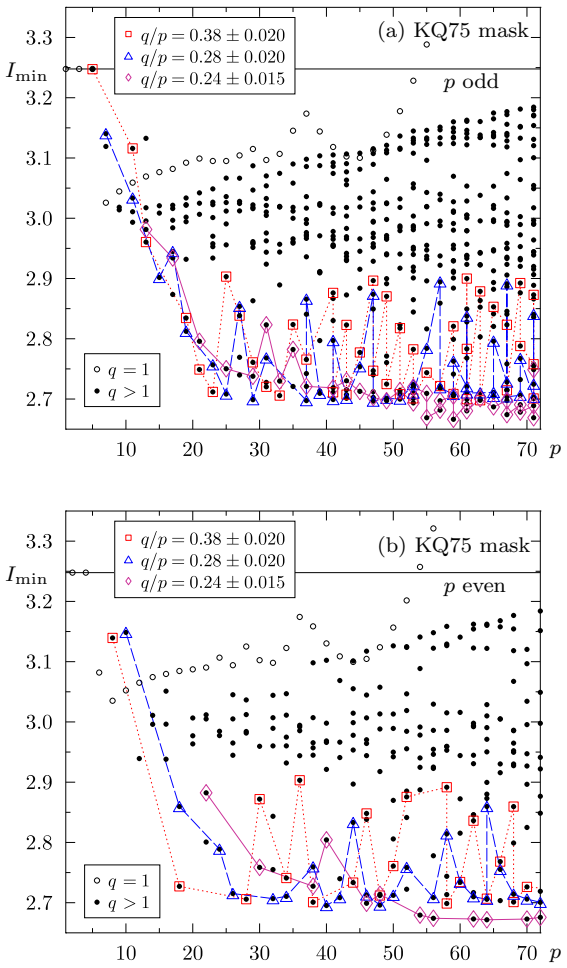

Figure 7. The minima $I_{\min}$ of the I statistics are shown as in figure 5. However, $C^{\text{obs}}(\vartheta)$ is obtained from the WMAP ILC 7yr map by applying the KQ75 mask.

$\Omega_{\text{tot}} = 1.02$, these lens spaces provide an alternative worth for follow-up studies.

ACKNOWLEDGMENTS

We would like to thank the Deutsche Forschungsgemeinschaft for financial support (AU 169/1-1). HEALPix [healpix.jpl.nasa.gov] (Górski et al. 2005) and the WMAP data from the LAMBDA website (lambda.gsfc.nasa.gov) were used in this work.

REFERENCES

Aurich, R., Janzer, H. S., Lustig, S., and Steiner, F. (2008). Do we Live in a "Small Universe"? *Class. Quantum Grav.*, 25:125006.

Aurich, R., Kramer, P., and Lustig, S. (2011). CMB radiation in an inhomogeneous spherical space. *Physica Scripta*, 84:055901.

Aurich, R. and Lustig, S. (2011). Can one reconstruct the masked CMB sky? *Mon. Not. R. Astron. Soc.*, 411:124–136.

Aurich, R. and Lustig, S. (2012). How well-proportioned are lens and prism spaces? *arXiv:1201.6490 [astro-ph.CO]*.

Aurich, R., Lustig, S., and Steiner, F. (2005). CMB anisotropy of spherical spaces. *Class. Quantum Grav.*, 22:3443–3459.

Bennett, C. L., Hill, R. S., Hinshaw, G., Larson, D., Smith, K. M., Dunkley, J., Gold, B., Halpern, M., Jarosik, N., Kogut, A., Komatsu, E., Limon, M., Meyer, S. S., Nolta, M. R., Odegard, N., Page, L., Spergel, D. N., Tucker, G. S., Weiland, J. L., Wollack, E., and Wright, E. L. (2011). Seven-Year Wilkinson Microwave Anisotropy

Probe (WMAP) Observations: Are There Cosmic Microwave Background Anomalies? *Astrophys. J. Supp.*, 192:17.

Copi, C. J., Huterer, D., Schwarz, D. J., and Starkman, G. D. (2009). No large-angle correlations on the non-Galactic microwave sky. *Mon. Not. R. Astron. Soc.*, 399:295–303.

Copi, C. J., Huterer, D., Schwarz, D. J., and Starkman, G. D. (2010). Large angle anomalies in the CMB. *Adv. Astron.*, 2010:847541.

Copi, C. J., Huterer, D., Schwarz, D. J., and Starkman, G. D. (2011). Bias in low-multipole CMB reconstructions. *Mon. Not. R. Astron. Soc.*, 418:505–515.

Efstathiou, G., Ma, Y.-Z., and Hanson, D. (2010). Large-Angle Correlations in the Cosmic Microwave Background. *Mon. Not. R. Astron. Soc.*, 407:2530–2542.

Gausmann, E., Lehoucq, R., Luminet, J.-P., Uzan, J.-P., and Weeks, J. (2001). Topological lensing in spherical spaces. *Class. Quantum Grav.*, 18:5155–5186.

Gold, B., Odegard, N., Weiland, J. L., Hill, R. S., Kogut, A., Bennett, C. L., Hinshaw, G., Chen, X., Dunkley, J., Halpern, M., Jarosik, N., Komatsu, E., Larson, D., Limon, M., Meyer, S. S., Nolta, M. R., Page, L., Smith, K. M., Spergel, D. N., Tucker, G. S., Wollack, E., and Wright, E. L. (2011). Seven-Year Wilkinson Microwave Anisotropy Probe (WMAP) Observations: Galactic Foreground Emission. *Astrophys. J. Supp.*, 192:15.

Górski, K. M., Hivon, E., Banday, A. J., Wandelt, B. D., Hansen, F. K., Reinecke, M., and Bartelmann, M. (2005). HEALPix: A Framework for High-Resolution Discretization and Fast Analysis of Data Distributed on the Sphere. *Astrophys. J.*, 622:759–771. HEALPix web-site: http://healpix.jpl.nasa.gov/.

Hinshaw, G., Banday, A. J., Bennett, C. L., Górski, K. M., Kogut, A., Lineweaver, C. H., Smoot, G. F., and Wright, E. L. (1996). Two-Point Correlations in the COBE DMR Four-Year Anisotropy Maps. *Astrophys. J. Lett.*, 464:L25–L28.

Lachièze-Rey, M. and Luminet, J.-P. (1995). Cosmic topology. *Physics Report*, 254:135–214.

Levin, J. (2002). Topology and the cosmic microwave background. *Physics Report*, 365:251–333.

Luminet, J.-P. (2008). The Shape and Topology of the Universe. *arXiv:0802.2236 [astro-ph]*.

Luminet, J.-P. and Roukema, B. F. (1999). Topology of the Universe: Theory and Observation. In *NATO ASIC Proc. 541: Theoretical and Observational Cosmology*, page 117.

Rebouças, M. J. and Gomero, G. I. (2004). Cosmic Topology: a Brief Overview. *Braz. J. Phys.*, 34:1358–1366.

Spergel, D. N., Verde, L., Peiris, H. V., Komatsu, E., Nolta, M. R., Bennett, C. L., Halpern, M., Hinshaw, G., Jarosik, N., Kogut, A., Limon, M., Meyer, S. S., Page, L., Tucker, G. S., Weiland, J. L., Wollack, E., and Wright, E. L. (2003). First-Year Wilkinson Microwave Anisotropy Probe (WMAP) Observations: Determination of Cosmological Parameters. *Astrophys. J. Supp.*, 148:175–194.

Uzan, J.-P., Riazuelo, A., Lehoucq, R., and Weeks, J. (2004). Cosmic microwave background constraints on lens spaces. *Phys. Rev. D*, 69:043003–1–4.